CAMBRIDGE
UNIVERSITY PRESS

Article

Natromarkeyite and pseudomarkeyite, two new calcium uranyl carbonate minerals from the Markey mine, San Juan County, Utah, USA

Anthony R. Kampf[1]* , Travis A. Olds[2], Jakub Plášil[3], Peter C. Burns[4] and Joe Marty[5]

[1]Mineral Sciences Department, Natural History Museum of Los Angeles County, 900 Exposition Boulevard, Los Angeles, CA 90007, USA; [2]Section of Minerals and Earth Sciences, Carnegie Museum of Natural History, 4400 Forbes Avenue, Pittsburgh, Pennsylvania 15213, USA; [3]Institute of Physics ASCR, v.v.i., Na Slovance 1999/2, 18221 Prague 8, Czech Republic; [4]Department of Civil and Environmental Engineering and Earth Sciences, University of Notre Dame, Notre Dame, IN 46556, USA; and [5]5199 East Silver Oak Road, Salt Lake City, UT 84108, USA

Abstract

The new minerals natromarkeyite, $Na_2Ca_8(UO_2)_4(CO_3)_{13}(H_2O)_{24} \cdot 3H_2O$ (IMA2018-152) and pseudomarkeyite, $Ca_8(UO_2)_4(CO_3)_{12}$ $(H_2O)_{18} \cdot 3H_2O$ (IMA2018-114) were found in the Markey mine, San Juan County, Utah, USA, where they occur as secondary phases on asphaltum. Natromarkeyite properties are: untwinned blades and tablets to 0.2 mm, pale yellow green colour; transparent; white streak; bright bluish white fluorescence (405 nm laser); vitreous to pearly lustre; brittle; Mohs hardness 1½ to 2; irregular fracture; three cleavages ({001} perfect, {100} and {010} good); density = 2.70(2) g cm^{-3}; biaxial (–) with $\alpha = 1.528(2)$, $\beta = 1.532(2)$ and $\gamma = 1.533(2)$; and pleochroism is X = pale green yellow, Y ≈ Z = light green yellow. Pseudomarkeyite properties are: twinned tapering blades and tablets to 1 mm; pale green yellow colour; transparent; white streak; bright bluish white fluorescence (405 nm laser); vitreous to pearly lustre; brittle; Mohs hardness ≈ 1; stepped fracture; three cleavages ({10$\bar{1}$} very easy, {010} good, {100} fair); density = 2.88(2) g cm^{-3}; biaxial (–) with $\alpha = 1.549(2)$, $\beta = 1.553(2)$ and $\gamma = 1.557(2)$; and it is nonpleochroic. The Raman spectra of markeyite, natromarkeyite and pseudomarkeyite are very similar and exhibit bands consistent with UO_2^{2+}, CO_3^{2-} and O–H. Electron microprobe analyses provided the empirical formula $Na_{2.01}Ca_{7.97}Mg_{0.03}Cu_{0.05}^{2+}(UO_2)_4(CO_3)_{13}(H_2O)_{24} \cdot 3H_2O$ (–0.11 H) for natromarkeyite and $Ca_{7.95}(UO_2)_4$ $(CO_3)_{12}(H_2O)_{18} \cdot 3H_2O$ (+0.10 H) for pseudomarkeyite. Natromarkeyite is orthorhombic, *Pmmn*, $a = 17.8820(13)$, $b = 18.3030(4)$, $c = 10.2249(3)$ Å, $V = 3336.6(3)$ Å^3 and $Z = 2$. Pseudomarkeyite is monoclinic, $P2_1/m$, $a = 17.531(3)$, $b = 18.555(3)$, $c = 9.130(3)$ Å, $\beta = 103.95(3)°$, $V = 2882.3(13)$ Å^3 and $Z = 2$. The structures of natromarkeyite ($R_1 = 0.0202$ for 2898 $I > 2\sigma I$) and pseudomarkeyite ($R_1 = 0.0787$ for 2106 $I > 2\sigma I$) contain uranyl tricarbonate clusters that are linked by (Ca/Na)–O polyhedra forming thick corrugated heteropolyhedral layers. Natromarkeyite is isostructural with markeyite; pseudomarkeyite has a very similar structure.

Introduction

The mines in the Red Canyon portion of the White Canyon district in south-eastern Utah have yielded many new minerals in recent years. Most of these are from the Blue Lizard mine on the east side of Red Canyon; however, the Green Lizard mine and the Giveaway–Simplot mine, also on the east side of Red Canyon, have yielded new species as well. The vast majority of these new species are uranyl sulfates and most, especially from the Blue Lizard mine, contain Na. None of the new mineral species from the mines on the east side of Red Canyon contain essential Ca or carbonate. The Markey mine, on the west side of Red Canyon, has also proven to be a prolific source of new minerals,

having thus far yielded nine, including natromarkeyite and pseudomarkeyite, described herein (Table 1). All of these contain uranyl, most contain carbonate and several contain Ca.

The new minerals and their names were approved by the Commission on New Minerals, Nomenclature and Classification of the International Mineralogical Association (IMA). Natromarkeyite (IMA2018-152, Kampf *et al*, 2019b) is named as a sodium analogue of markeyite, with two Na in place of one Ca in the structure. Pseudomarkeyite (IMA2018-114, Kampf *et al.*, 2019a) is named for its similarity to markeyite. The two minerals occur in intimate association and are similar in appearance, composition, Raman spectra and structure. Note that markeyite (/ma:r ′ki: ait/) is named for the locality, the Markey mine. The type specimens for both minerals are deposited in the collections of the Natural History Museum of Los Angeles County, 900 Exposition Boulevard, Los Angeles, CA 90007, USA. The description of natromarkeyite is based on one holotype and one cotype specimen with catalogue numbers 67487 (holotype) and 67488

Table 1. New minerals from the Markey mine.

Mineral	Formula	Reference
Feynmanite*	$Na_2(UO_2)_2(SO_4)_2(OH)_2(H_2O)_7$	[1]
Leószilárdite	$Na_2Mg(UO_2)_2(CO_3)_3(H_2O)_3$	[2]
Magnesioleydetite	$Mg(UO_2)(SO_4)_2(H_2O)_7 \cdot 4H_2O$	[3]
Markeyite	$Ca_9(UO_2)_4(CO_3)_{13}(H_2O)_{22} \cdot 6H_2O$	[4]
Meyrowitzite	$Ca_3(UO_2)_3(CO_3)_6(H_2O)_{10} \cdot 5H_2O$	[5]
Natromarkeyite	$Na_2Ca_8(UO_2)_4(CO_3)_{13}(H_2O)_{24} \cdot 3H_2O$	[6]
Pseudomarkeyite	$Ca_8(UO_2)_4(CO_3)_{12}(H_2O)_{18} \cdot 3H_2O$	[6]
Straßmannite§	$Al(UO_2)_2(SO_4)_2F(H_2O)_3 \cdot 13H_2O$	[3]
Uroxite†	$(UO_2)_2(C_2O_4)(OH)_2(H_2O)_2 \cdot H_2O$	[7]

*Cotype locality; also found at the Blue Lizard mine, San Juan County, Utah.
§Cotype locality; also found at the Green Lizard mine, San Juan County, Utah.
†Cotype locality; also found at the Burro mine, San Miguel County, Colorado.
References: [1] Kampf et al. (2019c); [2] Olds et al. (2017a); [3] Kampf et al. (2019d); [4] Kampf et al. (2018); [5] Kampf et al. (2019e); [6] This study; and [7] Kampf et al. (2020)

(cotype). The description of pseudomarkeyite is based on one holotype specimen, catalogue number 67091, which is also the holotype for markeyite.

Occurrence

Natromarkeyite and pseudomarkeyite were found underground in the Markey mine, Red Canyon, White Canyon District, San Juan County, Utah, USA (37°32′57″N, 110°18′08″W). The Markey mine is located ~1 km southwest of the Blue Lizard mine, on the east-facing side of Red Canyon, ~72 km west of the town of Blanding, Utah, and ~22 km southeast of Good Hope Bay on Lake Powell. The geology of the Markey Mine is quite similar to that of the Blue Lizard mine (Chenoweth, 1993; Kampf, et al., 2017), although the secondary mineralogy of the Markey mine is notably richer in carbonate phases. Underground gas measurements collected in 2016 using a hand-held Crowcon Gasman CO_2 monitor showed consistently elevated CO_2 levels at the Markey mine, averaging ~1000 ppm CO_2 with a maximum recorded value of 1600 ppm CO_2, levels considerably higher than at the nearby Blue Lizard mine where carbonate mineral species are less abundant. Higher CO_2 concentration at the Markey mine may be connected to an abundance of calcite present in the ores, released by the action of acidic waters derived from decaying sulfides.

The following information regarding the history and geology is taken largely from Chenoweth (1993). Jim Rigg of Grand Junction, Colorado began staking claims in Red Canyon in March of 1949. The Markey group of claims, staked by Rigg and others, was purchased by the Anaconda Copper Mining Company on June 1, 1951. After limited exploration and production, the mine closed in 1955. The mine was subsequently acquired from Anaconda by Calvin Black of Blanding, Utah under whose ownership the mine operated from 1960 to 1982 and was a leading producer in the district for nearly that entire period.

The uranium deposits in Red Canyon occur within the Shinarump member of the Upper Triassic Chinle Formation, in channels incised into the reddish-brown siltstones of the underlying Lower Triassic Moenkopi Formation. The Shinarump member consists of medium- to coarse-grained sandstone, conglomeratic sandstone beds and thick siltstone lenses. Ore minerals (uraninite, montroseite and coffinite) were deposited as replacements of wood and other organic material and as disseminations in the enclosing sandstone. Since the mine closed in

1982, oxidation of primary ores in the humid underground environment has produced a variety of secondary minerals, mainly carbonates and sulfates, as efflorescent crusts on the surfaces of mine walls.

Natromarkeyite and pseudomarkeyite are very rare minerals in the secondary mineral assemblage at the Markey mine. They both occur on asphaltum. Natromarkeyite is associated with andersonite, calcite, gypsum and another new calcium uranyl carbonate phase that is currently under study. Pseudomarkeyite is associated with calcite, gypsum, markeyite (Kampf et al., 2017) and natrozippeite.
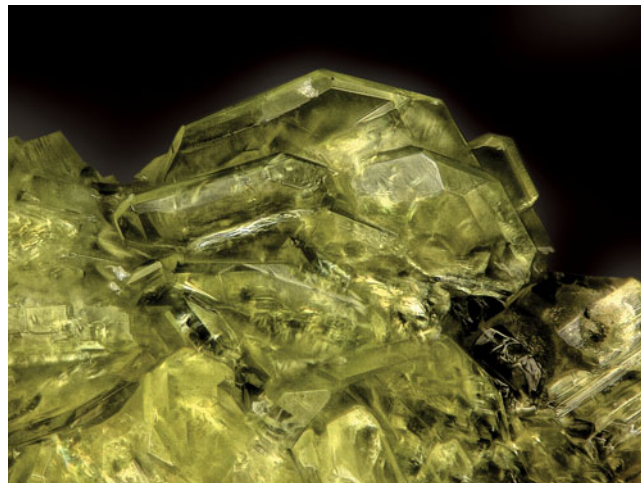
Physical and optical properties

Natromarkeyite

Natromarkeyite crystals are blades and tablets (Fig. 1) up to ~0.2 mm in maximum dimension, flattened on {001} and elongated on [100]. Crystals exhibit the forms {100}, {010}, {001}, {110}, {101}, {011} and {111} (Fig. 2). No twinning was observed.

Crystals are pale yellow green and transparent with vitreous to pearly lustre. The streak is white. The mineral fluoresces bright bluish white under a 405 nm laser. The Mohs hardness is between 1½ and 2, based upon scratch tests. Crystals are brittle with irregular fracture and three cleavages: perfect on {001}, good on {100} and {010}. At room temperature, the mineral dissolves very slowly in H_2O (minutes) and dissolves immediately with effervescence in dilute HCl. The density measured by flotation in a mixture of methylene iodide and toluene is 2.70(2) g cm^{-3}. The calculated density based on the empirical formula and unit-cell parameters obtained from single-crystal X-ray diffraction data is 2.695 g cm^{-3}.

Optically, natromarkeyite is biaxial (–), with $\alpha = 1.528(2)$, $\beta = 1.532(2)$ and $\gamma = 1.533(2)$ (measured in white light). The 2V, measured using extinction data collected on a spindle stage and analysed using EXCALIBRW (Gunter et al., 2004), is 46.5(7)°; the calculated 2V is 53.0°. Dispersion is $r > v$, weak. The mineral is weakly pleochroic: X = pale green yellow, $Y \approx Z$ = light green yellow; $X < Y \approx Z$. The optical orientation is $X = \mathbf{b}$, $Y = \mathbf{a}$ and $Z = \mathbf{c}$. The Gladstone–Dale compatibility index $1 - (K_P/K_C)$ for the empirical formula is –0.015, in the superior range (Mandarino, 2007), using $k(UO_3) = 0.118$, as provided by Mandarino (1976).

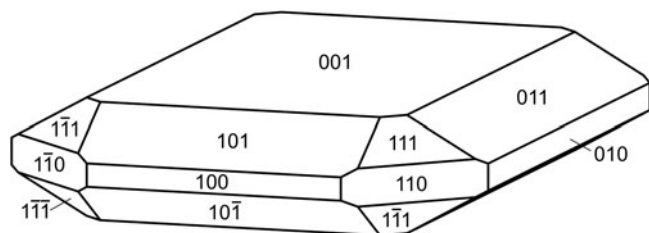**Fig. 1.** Natromarkeyite crystals on holotype specimen (#67487); FOV 0.4 mm across.

Fig. 2. Crystal drawing of natromarkeyite; clinographic projection in standard orientation.

Pseudomarkeyite

Pseudomarkeyite crystals are tapering blades and tablets (Fig. 3) up to ~1 mm in maximum dimension, flattened on $\{10\bar{1}\}$ and elongated on [010]. Crystals exhibit the forms $\{10\bar{1}\}$, $\{100\}$, $\{010\}$ and $\{510\}$; the $\{100\}$ and $\{510\}$ forms are based upon observed morphology, but were not measured. Twinning is ubiquitous, by 180° rotation about [101] (Fig. 4).

Crystals are pale green yellow and transparent with vitreous to pearly lustre. The streak is white. The mineral fluoresces bright bluish white under a 405 nm laser. The Mohs hardness is ~1, based upon scratch tests. Crystals are brittle with stepped fracture. Cleavage is perfect and very easy on $\{10\bar{1}\}$, good on $\{010\}$ and fair on $\{100\}$. Pseudomarkeyite loses birefringence (presumably due to decomposition), but does not dissolve in room-temperature H_2O; it dissolves immediately with effervescence in dilute HCl. The density measured by flotation in a mixture of methylene iodide and toluene is 2.88(2) g cm^{-3}. The calculated density based on the empirical formula and unit-cell parameters obtained from single-crystal X-ray diffraction data is 2.877 g cm^{-3}.

Optically, pseudomarkeyite is biaxial (–), with $\alpha = 1.549(2)$, $\beta = 1.553(2)$ and $\gamma = 1.557(2)$ (measured in white light). The 2V measured directly on a spindle stage is 88(2)°; the calculated 2V is 89.8°. No dispersion was observed and the mineral is nonpleochroic. The optical orientation is $Y = \mathbf{b}$, $Z \wedge \mathbf{a} = 30°$ in obtuse β ($X \approx \perp \{10\bar{1}\}$). The Gladstone–Dale compatibility index $1 - (K_P/K_C)$ for the empirical formula is –0.024, in the excellent range (Mandarino, 2007), using $k(UO_3) = 0.118$, as provided by Mandarino (1976).
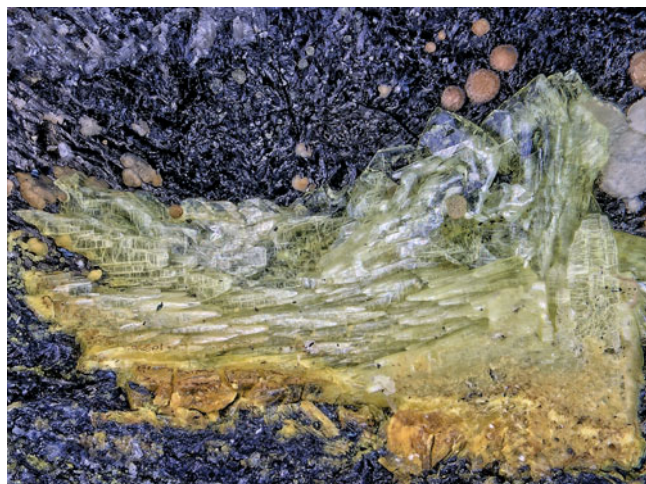
Fig. 3. Pseudomarkeyite (pearly tapering blades) and markeyite (lustrous blades in upper right) with calcite (brown and grey balls) on asphaltum on the holotype specimen (#67091); FOV 3.5 mm across.
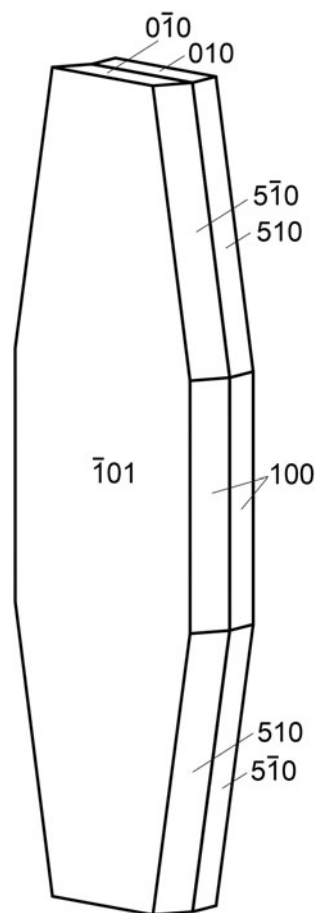
Fig. 4. Crystal drawing of pseudomarkeyite twin; clinographic projection in non-standard orientation, $\mathbf{b}$ vertical.

Raman spectroscopy

Raman spectroscopy was conducted on a Horiba XploRA PLUS using a 532 nm diode laser. The Raman spectra of natromarkeyite, pseudomarkeyite and markeyite are very similar. The spectra are compared in Fig. 5 and the bands are listed in Table 2 with their likely band assignments.

The broad multiple bands in the 3700–3100 cm^{-1} range are attributed to ν O–H stretching vibrations of structurally non-equivalent/symmetrically distinct hydrogen-bonded H_2O groups. According to the correlation given by Libowitzky (1999), this corresponds to approximate O–H···O hydrogen bond-lengths between 3.2 and 2.7 Å, which is consistent with what we report in the structure determinations. The broad bands in the 2800–2300 cm^{-1} range in the markeyite and pseudomarkeyite spectra were originally interpreted as corresponding to strong (short) hydrogen bonds (Kampf et al., 2018); however, no such bonds appear to exist in the structures of markeyite, natromarkeyite or pseudomarkeyite. We now think that this is a spectral artefact because we have also observed it in spectra of anhydrous minerals and we have recorded other spectra for markeyite that do not exhibit this feature. It is also possible that a small amount of asphaltum adhering to the crystals caused the bands in this region.

The weak bands between 1439 and 1358 cm^{-1} can be attributed to the ν_3 $(CO_3)^{2-}$ antisymmetric stretching vibrations of the $(CO_3)^{2-}$ units. Medium to strong multiple bands between 1094

Fig. 5. The Raman spectra of markeyite, natromarkeyite and pseudomarkeyite.

Table 2. Raman bands and mode assignments for markeyite, natromarkeyite and pseudomarkeyite.

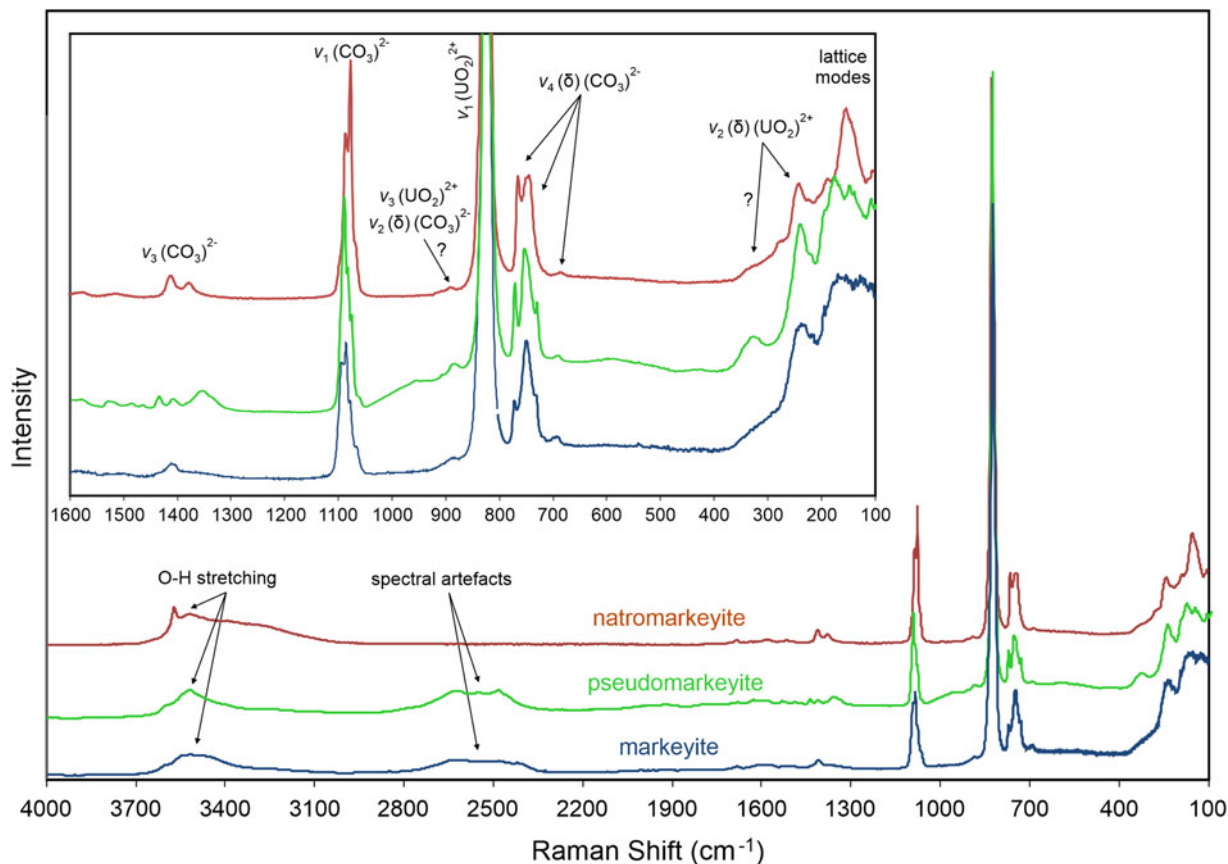| Markeyite	Natromarkeyite	Pseudomarkeyite	Vibrational modes
3700–3300	3700–3100	3700–3300	ν O–H stretching
2800–2300		2800–2300	spectral artefacts
		1439	ν_3 $(CO_3)^{2-}$ asym. stretching
1410	1413	1413	
	1379	1358	
1094		1093	ν_1 $(CO_3)^{2-}$ sym. stretching
1086	1087	1086	
1078	1078	1079	
1067	1069		
888	893	884	ν_2 (δ) $(CO_3)^{2-}$ bending or ν_3 $(UO_2)^{2+}$ asym. stretching
825	829	826	ν_1 $(UO_2)^{2+}$ sym. stretching
772		773	ν_4 (δ) $(CO_3)^{2-}$ bending (doubly degenerate)
750	752	756	
733	746	732	
698			
691	688	691	
318	336	326	ν_2 (δ) $(UO_2)^{2+}$ bending (split doubly degenerate)
238	243	238	
170	189	174	lattice modes
155	155	154	
127		137	

and 1067 cm^{-1} are connected with the ν_1 $(CO_3)^{2-}$ symmetric stretching vibrations of several structurally non-equivalent carbonate units (Koglin *et al.*, 1979; Anderson *et al.*, 1980; Čejka, 1999, 2005).

A weak band near 900 cm^{-1} may be due to the ν_2 (δ) $(CO_3)^{2-}$ bending vibrations or to the ν_3 $(UO_2)^{2+}$ antisymmetric stretching vibration; an overlap/coincidence of these two bands is possible. The very strong bands centred at 825, 829 and 826 cm^{-1} for markeyite, natromarkeyite and pseudomarkeyite are due to the ν_1 $(UO_2)^{2+}$ symmetric stretching vibrations and provide inferred U–O bond lengths around 1.78–1.79 Å (Bartlett and Cooney, 1989). The ν_2 (δ) $(CO_3)^{2-}$ bending vibration may coincide with this band.

Several weak to strong bands between 773 and 688 cm^{-1} are assigned to the doubly degenerate ν_4 (δ) $(CO_3)^{2-}$ bending vibrations. The medium broad band in the spectra centred near 240 cm^{-1} is assigned to the split doubly degenerate ν_2 (δ) $(UO_2)^{2+}$ bending vibrations. Bands between 189 and 127 cm^{-1} are due to lattice modes (Koglin *et al.*, 1979; Anderson *et al.*, 1980; Čejka, 1999, 2005).

Chemical composition

Chemical analyses (five for natromarkeyite and eight for pseudomarkeyite) were performed using a JEOL JXA-8230 electron microprobe operated in wavelength dispersive mode at 15 kV and 1 nA, with a 10 μm beam diameter. Matrix effects were accounted for using the *PAP* correction routine (Pouchou and Pichoir, 1991). For natromarkeyite, a time-dependent intensity correction was applied to Na. H_2O and CO_2 were not determined

Table 3. Chemical composition (in wt.%) for natromarkeyite and pseudomarkeyite.

Oxide	Natromarkeyite				Pseudomarkeyite				Standard
	Mean	Range	S.D.	Ideal	Mean	Range	S.D.	Ideal	
Na_2O	2.35	2.05–2.67	0.30	2.28	bdl				Albite
CaO	16.90	16.13–17.55	0.62	16.53	17.81	17.37–18.41	0.34	17.95	Wollastonite
MgO	0.04	0.00–0.14	0.06		bdl				Synthetic MgO
CuO	0.15	0.00–0.36	0.15		bdl				Chalcopyrite
UO_3	43.25	41.36–45.39	1.55	42.17	45.73	44.01–47.43	1.25	45.78	Synthetic UO_2
CO_2*	21.63			21.09	21.11			21.13	
H_2O*	18.35			17.93	15.16			15.14	
Total	102.67				99.81				

* Based on the structure.
bdl: below detection limit; S.D. standard deviation.

directly because of extreme paucity of material. The H_2O and CO_2 contents were calculated by stoichiometry in accord with the crystal structure determinations: based on 4 U, 13 C and 74 O atoms per formula unit (apfu) for natromarkeyite and 4 U, 12 C and 65 O apfu for pseudomarkeyite. The high analytical total for natromarkeyite is presumably due to the loss of loosely bound H_2O under vacuum resulting in higher concentrations for the remaining constituents than are to be expected for the fully hydrated phase. Analytical data are given in Table 3. No other elements with atomic numbers higher than 8 were above the detection limits.

The empirical formula for natromarkeyite (calculated on the basis of 74 O apfu) is $Na_{2.01}Ca_{7.97}Mg_{0.03}Cu_{0.05}U_{4.00}C_{13.00}O_{74.00}$ $H_{53.89}$ or $Na_{2.01}Ca_{7.97}Mg_{0.03}Cu_{0.05}(UO_2)_4(CO_3)_{13}(H_2O)_{24}·3H_2O$

(–0.11 H). The ideal formula is $Na_2Ca_8(UO_2)_4(CO_3)_{13}(H_2O)_{24}·$ $3H_2O$. The empirical formula for pseudomarkeyite (calculated on the basis of 65 O apfu) is $Ca_{7.95}U_{4.00}C_{12.00}O_{65.00}H_{42.11}$, or $Ca_{7.95}(UO_2)_4(CO_3)_{12}(H_2O)_{18}·3H_2O$ (+0.10 H). The ideal formula is $Ca_8(UO_2)_4(CO_3)_{12}·21H_2O$.

X-ray crystallography and structure refinement

Powder X–ray diffraction studies were done using a Rigaku R–Axis Rapid II curved imaging plate microdiffractometer, with monochromatised MoKα radiation (λ = 0.71075 Å). A Gandolfi-like motion on the φ and ω axes was used to randomise the samples and observed *d* values and intensities were derived by profile fitting

Table 4. Data collection and structure refinement details for natromarkeyite and pseudomarkeyite.*

	Natromarkeyite	Pseudomarkeyite
Crystal data		
Structural formula	$Na_2Ca_8(UO_2)_4(CO_3)_{13}(H_2O)_{24}·3H_2O$	$Ca_8(UO_2)_4(CO_3)_{12}(H_2O)_{18}·3H_2O$
Space group	*Pmmn*	*P2₁/m*
Unit-cell dimensions (Å, °)	$a = 17.8820(13)$	$a = 17.531(3)$
	$b = 18.3030(4)$	$b = 18.555(3)$
	$c = 10.2249(3)$	$c = 9.130(3)$
		$β = 103.95(3)$
V (Å³)	3346.6(3)	2882.3(13)
Z	2	2
Density (above formula) (g cm⁻³)	2.693	2.880
Absorption coefficient (mm⁻¹)	10.419	12.059
Data collection		
Diffractometer	Rigaku R-Axis Rapid II	Rigaku R-Axis Rapid II
X-ray radiation/power	MoKα (λ = 0.71075 Å)/50 kV, 40 mA	MoKα (λ = 0.71075 Å)/50 kV, 40 mA
Temperature (K)	293(2)	293(2)
Crystal size (μm)	100 × 100 × 30	120 × 70 × 30
F(000)	2548	2324
θ range (°)	3.20 to 25.03	3.04 to 19.96
Index ranges	$−21 \leq h \leq 21$	$−16 \leq h \leq 16$
	$−21 \leq k \leq 21$	$−17 \leq k \leq 16$
	$−12 \leq l \leq 12$	$−8 \leq l \leq 8$
Reflections collected/unique	20715/3150; $R_{int} = 0.034$	11253/2772; $R_{int} = 0.12$
Reflections with $I > 2σI$	2898	2106
Completeness to $θ_{max}$ (%)	99.4	99.5
Max./min. transmission	0.745/0.422	0.714/0.326
Refinement		
Refinement method	Full-matrix least-squares on F^2	Full-matrix least-squares on F^2
Parameters/restraints	309/21	226/0
GoF	1.045	1.055
Final *R* indices [$I > 2σI$]	$R_1 = 0.0202$, $wR_2 = 0.0442$	$R_1 = 0.0787$, $wR_2 = 0.2015$
R indices (all data)	$R_1 = 0.0234$, $wR_2 = 0.0453$	$R_1 = 0.1023$, $wR_2 = 0.2267$
Largest diff. peak/hole (e^- A⁻³)	+1.58/−0.67	+4.45/−1.74

*$R_{int} = Σ|F_o^2−F_o^2(mean)|/Σ[F_o^2]$. GoF = $S = \{Σ[w(F_o^2−F_c^2)^2]/(n−p)\}^{½}$. $R_1 = Σ||F_o|−|F_c||/Σ|F_o|$. $wR_2 = \{Σ[w(F_o^2−F_c^2)^2]/Σ[w(F_o^2)^2]\}^{½}$; $w = 1/[σ^2(F_o^2)+(aP)^2+bP]$ where P is $[2F_c^2+Max(F_o^2,0)]/3$; for natromarkeyite, *a* is 0.0201 and *b* is 9.22; for pseudomarkeyite, *a* is 0.1226 and *b* is 100.5513.

Table 5. Atom coordinates, displacement parameters (Å^2) and site occupancies for natromarkeyite.

	x/a	y/b	z/c	U_{eq}	Occ.	U^{11}	U^{22}	U^{33}	U^{23}	U^{13}	U^{12}
U1	0.46930(2)	¾	0.99124(2)	0.01533(7)	1	0.01778(11)	0.01168(11)	0.01652(12)	0	−0.00316(8)	0
U2	¼	0.46718(2)	0.07581(2)	0.01935(7)	1	0.01172(11)	0.02721(12)	0.01913(13)	−0.00579(9)	0	0
Ca1	0.44003(4)	0.43571(4)	0.87349(8)	0.01445(17)	1	0.0126(4)	0.0130(4)	0.0177(4)	−0.0009(3)	−0.0001(3)	0.0011(3)
Ca2	0.38124(5)	0.63974(5)	0.60892(8)	0.02310(19)	1	0.0238(4)	0.0239(4)	0.0216(5)	−0.0029(3)	−0.0033(4)	0.0054(4)
Na1	¼	¼	0.6853(2)	0.0437(10)	1	0.051(2)	0.0174(17)	0.062(3)	0	0	0
Na2	¼	¾	0.1043(5)	0.091(2)	1	0.030(2)	0.209(7)	0.034(3)	0	0	0
C1	0.4269(2)	0.6130(2)	0.8739(4)	0.0177(8)	1	0.019(2)	0.0146(19)	0.019(2)	−0.0014(16)	−0.0013(17)	0.0005(17)
C2	0.6095(2)	0.4928(2)	0.8074(4)	0.0205(9)	1	0.017(2)	0.024(2)	0.020(2)	−0.0003(17)	−0.0009(17)	−0.0003(18)
C3	¼	0.4033(3)	0.8191(6)	0.0234(13)	1	0.017(3)	0.029(3)	0.024(4)	−0.005(3)	0	0
C4	0.4388(4)	¼	0.7774(7)	0.0357(17)	1	0.050(4)	0.020(3)	0.037(4)	0	−0.026(4)	0
C5	¼	0.7232(6)	0.5850(12)	0.023(3)	0.5	0.024(6)	0.017(5)	0.027(7)	−0.001(4)	0	0
O1	0.40941(15)	0.55646(14)	0.8130(3)	0.0215(6)	1	0.0283(15)	0.0119(13)	0.0245(16)	−0.0027(12)	−0.0054(12)	0.0022(12)
O2	0.46666(15)	0.61501(15)	0.9792(3)	0.0227(7)	1	0.0293(16)	0.0163(14)	0.0226(17)	0.0000(12)	−0.0118(13)	0.0009(12)
O3	0.40536(17)	0.67674(14)	0.8303(3)	0.0250(7)	1	0.0411(17)	0.0108(13)	0.0230(17)	−0.0017(12)	−0.0145(14)	0.0014(13)
O4	0.55004(14)	0.46709(15)	0.7591(3)	0.0227(6)	1	0.0127(13)	0.0341(16)	0.0212(16)	−0.0014(13)	−0.0015(12)	−0.0025(13)
O5	0.67282(15)	0.48721(18)	0.7470(3)	0.0306(7)	1	0.0140(13)	0.056(2)	0.0220(17)	−0.0126(15)	0.0027(12)	−0.0041(14)
O6	0.38786(15)	0.47324(16)	0.0820(3)	0.0236(7)	1	0.0167(14)	0.0358(17)	0.0183(16)	−0.0072(13)	0.0010(12)	−0.0006(13)
O7	¼	0.3766(2)	0.7067(4)	0.0310(10)	1	0.024(2)	0.045(3)	0.024(3)	−0.013(2)	0	0
O8	0.31061(15)	0.41739(18)	0.8838(3)	0.0289(7)	1	0.0130(13)	0.0475(19)	0.0260(18)	−0.0146(15)	0.0006(12)	−0.0007(14)
O9	0.4025(4)	¼	0.6754(6)	0.082(3)	1	0.161(7)	0.023(3)	0.062(4)	0	−0.084(5)	0
O10	0.46009(18)	0.30954(15)	0.8378(3)	0.0309(8)	1	0.047(2)	0.0146(14)	0.0309(18)	−0.0013(13)	−0.0214(15)	0.0014(14)
O11	0.3875(2)	¾	0.0924(4)	0.0287(10)	1	0.027(2)	0.030(2)	0.029(3)	0	0.0025(19)	0
O12	0.5497(2)	¾	0.8901(5)	0.0336(11)	1	0.028(2)	0.034(2)	0.038(3)	0	0.012(2)	0
O13	¼	0.3783(2)	0.1463(5)	0.0340(11)	1	0.030(2)	0.032(2)	0.040(3)	0.007(2)	0	0
O14	¼	0.5567(2)	0.0074(4)	0.0313(10)	1	0.028(2)	0.031(2)	0.035(3)	−0.001(2)	0	0
O15	0.3132(2)	¾	0.5731(5)	0.0292(10)	1	0.017(2)	0.031(2)	0.040(3)	0	0.0021(19)	0
O16	¼	0.6545(5)	0.6237(10)	0.034(2)	0.5	0.021(4)	0.021(4)	0.059(7)	0(4)	0	0
OW1	0.3291(2)	0.52893(18)	0.5187(3)	0.0351(8)	1	0.050(2)	0.0341(18)	0.0217(18)	−0.0025(15)	−0.0062(16)	0.0050(16)
H1A	0.328(3)	0.526(3)	0.4379(19)	0.042	1						
H1B	0.360(2)	0.499(2)	0.539(4)	0.042	1						
OW2	0.40387(18)	0.41062(18)	0.6402(3)	0.0337(8)	1	0.0404(19)	0.0338(18)	0.0269(19)	−0.0007(16)	−0.0066(15)	0.0053(16)
H2A	0.395(2)	0.3682(10)	0.635(5)	0.040	1						
H2B	0.3675(18)	0.433(2)	0.620(5)	0.040	1						
OW3	¼	0.6651(3)	0.2660(7)	0.0655(18)	1	0.049(3)	0.040(3)	0.107(6)	−0.015(3)	0	0
H3A	¼	0.6212(11)	0.267(7)	0.079	1						
H3B	¼	0.680(4)	0.340(4)	0.079	1						
OW4	0.4013(2)	0.6617(2)	0.3763(3)	0.0417(9)	1	0.052(2)	0.043(2)	0.030(2)	−0.0039(16)	0.0057(17)	0.0078(18)
H4A	0.416(3)	0.629(2)	0.330(4)	0.050	1						
H4B	0.3633(19)	0.677(3)	0.344(5)	0.050	1						
OW5	0.4764(3)	¾	0.5880(6)	0.0415(12)	1	0.033(3)	0.043(3)	0.049(3)	0	0.000(2)	0
H5A	0.495(4)	¾	0.514(3)	0.050	1						
H5B	0.509(4)	0.728(5)	0.631(6)	0.050	0.5						
OW6	0.4995(2)	0.5811(2)	0.5816(4)	0.0484(10)	1	0.041(2)	0.055(2)	0.049(2)	0.024(2)	0.0172(19)	0.0213(19)
H6A	0.513(3)	0.5426(17)	0.614(6)	0.058	1						
H6B	0.535(2)	0.607(2)	0.578(6)	0.058	1						
OW7	¼	0.6247(4)	0.7372(8)	0.0192(17)	0.5	0.022(4)	0.016(4)	0.020(5)	0.002(3)	0	0
H7A	¼	0.660(3)	0.787(7)	0.023	0.5						
H7B	¼	0.588(3)	0.783(8)	0.023	0.5						
OW8	¼	¾	0.8832(7)	0.0428(18)	1	0.029(3)	0.075(5)	0.025(4)	0	0	0
OW9	¼	¼	0.9275(10)	0.115(5)	1	0.254(17)	0.044(5)	0.048(6)	0	0	0
OW10	0.6288(5)	0.6751(6)	0.6665(9)	0.154(6)	0.797(19)	0.116(8)	0.235(12)	0.110(8)	0.012(7)	−0.016(6)	−0.003(7)
OW11	¼	¼	0.4693(14)	0.213(16)	0.96(5)	0.123(15)	0.46(4)	0.053(10)	0	0	0

Anthony Kampf et al.

Table 6. Atom coordinates and displacement parameters (Å^2) for pseudomarkeyite.

	x/a	y/b	z/c	U_{eq}	U^{11}	U^{22}	U^{33}	U^{23}	U^{13}	U^{12}
Ca1	0.3218(4)	0.4523(4)	0.3212(7)	0.0446(18)	0.037(4)	0.053(5)	0.042(4)	0.001(3)	0.006(3)	0.001(3)
Ca2	0.0353(3)	0.5605(3)	0.6980(8)	0.0419(17)	0.032(4)	0.034(4)	0.057(5)	0.003(3)	0.006(3)	−0.001(3)
Ca3	0.1455(5)	¼	0.9299(11)	0.050(3)	0.045(6)	0.044(6)	0.055(7)	0	0.000(5)	0
Ca4	0.1983(5)	¾	0.0965(11)	0.046(3)	0.032(5)	0.029(5)	0.069(7)	0	−0.001(5)	0
Ca5	0.4234(3)	0.5655(3)	0.0674(7)	0.0371(16)	0.031(4)	0.030(4)	0.046(4)	−0.002(3)	0.001(3)	0.002(3)
U1	0.25997(7)	0.53908(7)	0.67504(14)	0.0418(5)	0.0346(9)	0.0441(9)	0.0440(10)	−0.0021(6)	0.0042(6)	−0.0001(6)
U2	0.52292(10)	¾	0.9815(2)	0.0408(6)	0.0365(11)	0.0362(11)	0.0491(13)	0	0.0093(9)	0
U3	0.97059(10)	¾	0.4935(2)	0.0457(6)	0.0418(12)	0.0367(12)	0.0529(13)	0	0.0003(9)	0
C1	0.2212(19)	0.5975(17)	0.937(4)	0.046(9)						
C2	0.4169(19)	0.4919(17)	0.697(4)	0.047(9)						
C3	0.1409(17)	0.5037(16)	0.410(4)	0.040(8)						
C4	0.4163(16)	0.3845(15)	0.086(3)	0.034(8)						
C5	0.389(3)	¾	0.125(6)	0.075(17)						
C6	0.051(2)	0.3833(19)	0.666(4)	0.059(10)						
C7	0.045(2)	¾	0.817(5)	0.039(11)						
O1	0.1690(11)	0.5831(10)	0.817(2)	0.040(5)						
O2	0.2906(12)	0.5777(11)	0.938(2)	0.049(6)						
O3	0.2045(11)	0.6246(11)	0.053(2)	0.042(5)						
O4	0.4789(12)	0.4585(10)	0.702(2)	0.044(6)						
O5	0.3649(11)	0.4992(10)	0.573(2)	0.042(5)						
O6	0.3991(10)	0.5254(10)	0.811(2)	0.033(5)						
O7	0.9072(14)	0.5221(13)	0.698(3)	0.064(7)						
O8	0.1235(10)	0.5321(9)	0.526(2)	0.033(5)						
O9	0.2172(12)	0.5065(12)	0.416(2)	0.054(6)						
O10	0.3868(12)	0.3258(12)	0.115(2)	0.053(6)						
O11	0.4708(11)	0.3827(11)	0.022(2)	0.041(5)						
O12	0.3884(12)	0.4457(11)	0.119(2)	0.045(6)						
O13	0.3325(17)	¾	0.176(3)	0.047(8)						
O14	0.4260(11)	0.6917(10)	0.096(2)	0.037(5)						
O15	0.9694(13)	0.6192(12)	0.473(3)	0.058(6)						
O16	0.0725(14)	0.3209(13)	0.734(3)	0.071(7)						
O17	0.0599(13)	0.4400(12)	0.754(3)	0.058(6)						
O18	0.0744(16)	¾	0.948(3)	0.044(8)						
O19	0.0213(13)	0.8074(12)	0.736(2)	0.057(6)						
O20	0.2755(11)	0.6294(10)	0.629(2)	0.042(5)						
O21	0.2454(12)	0.4476(12)	0.724(2)	0.055(6)						
O22	0.4555(17)	¾	0.804(3)	0.051(8)						
O23	0.5971(16)	¾	0.161(3)	0.044(8)						
O24	0.0633(17)	¾	0.460(3)	0.053(8)						
O25	0.8754(19)	¾	0.529(4)	0.065(10)						
OW1	0.4398(13)	0.3822(13)	0.444(3)	0.067(7)						
OW2	0.164(2)	0.6743(19)	0.301(4)	0.120(11)						
OW3	0.2101(14)	0.4536(13)	0.111(3)	0.067(7)						
OW4	0.2290(19)	¾	0.827(4)	0.069(10)						
OW5	0.3429(11)	0.5777(10)	0.260(2)	0.042(5)						
OW6	0.0427(13)	0.5698(13)	0.983(3)	0.064(7)						
OW7	0.2580(17)	0.3498(16)	0.408(3)	0.094(9)						
OW8	0.251(2)	¼	0.162(5)	0.096(13)						
OW9	0.243(2)	0.167(2)	0.904(5)	0.150(14)						
OW10	0.0902(19)	0.1658(17)	0.073(4)	0.109(10)						
OW11	0.4046(12)	0.6725(11)	0.496(2)	0.047(6)						
OW12	0.390(3)	¼	0.534(5)	0.104(14)						

using *JADE 2010* software (Materials Data, Inc.). The powder data are presented in Supplementary Tables S1 and S2 for natromarkeyite and pseudomarkeyite, respectively. These tables, along with the crystallographic information files, have been deposited with the Principal Editor of *Mineralogical Magazine* and are available as Supplementary material (see below).

The single-crystal structure data were collected at room temperature using the same diffractometer and radiation noted above. The selection of a crystal of natromarkeyite was straightforward because, despite their rarity, the natromarkeyite crystals are untwinned and of good quality for single-crystal study. Unfortunately, pseudomarkeyite crystals are invariably twinned (by rotation on [101]) and exhibit high mosaicity. These problems, coupled with the close

spacing of reflections due to the large *a* and *b* cell parameters, made the integration of reflections problematic. The best data were obtained from a twinned crystal with one larger twin component; however, it proved impossible to adequately separate the reflections from the smaller component during integration. In addition, relatively weak diffraction only provided data to 40°2θ.

For each mineral, single-crystal data were processed using the Rigaku *CrystalClear* software package and an empirical (multi–scan) absorption correction was applied using the *ABSCOR* program (Higashi, 2001) in the *CrystalClear* software suite. The structures were solved by direct methods using *SIR2011* (Burla *et al.*, 2012). *SHELXL-2016* (Sheldrick, 2015) was used for the structure refinements.

Table 7. Selected bond distances (Å) and angles (°) for natromarkeyite.

U1–O12	1.771(4)	Ca2–O16 ×½	2.3671(15)	C1–O1	1.247(5)
U1–O11	1.791(4)	Ca2–O15	2.385(2)	C1–O2	1.292(5)
U1–O3 ×2	2.411(3)	Ca2–OW6	2.389(2)	C1–O3	1.306(5)
U1–O10 ×2	2.416(3)	Ca2–O3	2.402(3)	<C1–O>	1.282
U1–O2 ×2	2.474(3)	Ca2–OW1	2.416(3)		
<U1–O$_{ap}$>	1.781	Ca2–OW4	2.439(4)	C2–O4	1.263(5)
<U1–O$_{eq}$>	2.434	Ca2–O1	2.633(3)	C2–O6	1.291(5)
U2–O13	1.779(4)	Ca2–OW5	2.649(3)	C2–O5	1.294(5)
U2–O14	1.782(4)	Ca2–OW7 ×½	2.702(4)	<C2–O>	1.283
U2–O8 ×2	2.420(3)	<Ca2–O>	2.481		
U2–O5 ×2	2.426(3)			C3–O7	1.249(7)
U2–O6 ×2	2.469(3)	Na1–OW11	2.208(15)	C3–O8 ×2	1.296(4)
<U2–O$_{ap}$>	1.781	Na1–O7 ×2	2.327(5)	<C3–O>	1.280
<U2–O$_{eq}$>	2.438	Na1–OW9	2.477(11)		
Ca1–O8	2.341(3)	Na1–O9 ×2	2.729(8)	C4–O9	1.228(8)
Ca1–O1	2.359(3)	<Na1–O>	2.466	C4–O10 ×2	1.309(4)
Ca1–O4	2.360(3)			<C4–O>	1.282
Ca1–O10	2.365(3)	Na2–OW8	2.261(9)		
Ca1–O6	2.426(3)	Na2–OW3 ×2	2.269(7)	C5–O15 ×2	1.238(6)
Ca1–O2	2.432(3)	Na2–O11 ×2	2.462(4)	C5–O16	1.319(14)
Ca1–OW2	2.514(3)	<Na2–O>	2.345	<C5–O>	1.265
<Ca1–O>	2.400				

Hydrogen bonds (*D* = donor O, *A* = acceptor O)

D–H	D–H	H···A	D···A	<DHA	A
OW1–H1A	0.828(19)	1.90(2)	2.732(4)	176(5)	O5
OW1–H1B	0.811(19)	2.07(2)	2.832(5)	157(5)	OW2
OW2–H2A	0.794(19)	2.21(2)	2.962(4)	159(5)	O9
OW2–H2B	0.792(19)	2.50(2)	2.902(5)	113(4)	O7
OW3–H3A	0.80(2)	2.422(17)	3.114(6)	145(1)	O5 ×2*
OW3–H3B	0.81(2)				none
OW4–H4A	0.805(19)	2.07(2)	2.869(4)	170(6)	O4
OW4–H4B	0.806(19)	2.19(3)	2.933(5)	153(5)	OW3
OW5–H5A	0.83(2)				none
OW5–H5B	0.83(2)	2.38(4)	3.153(10)	155(7)	OW10
OW6–H6A	0.814(19)	2.13(3)	2.909(5)	159(6)	O4
OW6–H6B	0.797(19)	2.27(3)	3.010(11)	154(6)	OW10
OW7–H7A	0.82(2)	1.92(2)	2.736(8)	172(9)	OW8
OW7–H7B	0.81(2)	2.36(7)	3.030(9)	139(8)	O14
OW8			3.259(6)		O11
OW8			3.177(11)		O16
OW9			3.243(8)		O13 ×2
OW10			3.018(11)		O12
OW10			3.053(10)		O13
OW11			2.917(12)		OW10 ×2

* The H3B site is split into two symmetrically related, half-occupied sites, each of which bonds to an O5 atom.

Table 8. Selected bond distances (Å) for pseudomarkeyite.

Ca1–OW3	2.39(2)	C1–O3	1.27(3)	U1–O20	1.77(2)
Ca1–O5	2.40(2)	C1–O2	1.27(3)	U1–O21	1.79(2)
Ca1–O12	2.41(2)	C1–O1	1.28(3)	U1–O5	2.37(2)
Ca1–O9	2.42(2)	<C1–O>	1.27	U1–O9	2.38(2)
Ca1–OW7	2.43(3)			U1–O1	2.43(2)
Ca1–OW5	2.44(2)	C2–O4	1.24(3)	U1–O2	2.43(2)
Ca1–OW1	2.47(2)	C2–O5	1.28(3)	U1–O8	2.45(2)
<Ca1–O>	2.42	C2–O6	1.32(3)	U1–O6	2.47(2)
		<C2–O>	1.28	<U1–O$_{ap}$>	1.78
Ca2–O17	2.31(2)			<U1–O$_{eq}$>	2.42
Ca2–O7	2.36(2)	C3–O7	1.23(3)		
Ca2–O15	2.36(2)	C3–O8	1.29(3)	U2–O22	1.76(3)
Ca2–O1	2.37(2)	C3–O9	1.33(3)	U2–O23	1.83(3)
Ca2–O19	2.50(2)	<C3–O>	1.28	U2–O10 ×2	2.43(2)
Ca2–O8	2.51(2)			U2–O14 ×2	2.45(2)
Ca2–OW6	2.58(2)	C4–O11	1.23(3)	U2–O11 ×2	2.47(2)
<Ca2–O>	2.43	C4–O10	1.26(3)	<U2–O$_{ap}$>	1.80
		C4–O12	1.30(3)	<U2–O$_{eq}$>	2.45
Ca3–O16 ×2	2.34(3)	<C4–O>	1.26		
Ca3–OW9 ×2	2.35(4)			U3–O24	1.72(3)
Ca3–OW10 ×2	2.39(3)	C5–O13	1.19(6)	U3–O25	1.78(3)
Ca3–OW8	2.46(4)	C5–O14 ×2	1.32(4)	U3–O16 ×2	2.42(2)
<Ca3–O>	2.37	<C5–O>	1.28	U3–O19 ×2	2.42(2)
				U3–O15 ×2	2.43(2)
Ca4–O18	2.27(3)	C6–O15	1.23(4)	<U3–O$_{ap}$>	1.75
Ca4–O13	2.29(3)	C6–O17	1.31(4)	<U3–O$_{eq}$>	2.42
Ca4–O3 ×2	2.37(2)	C6–O16	1.32(4)		
Ca4–OW2 ×2	2.52(3)	<C6–O>	1.29		
Ca4–OW4	2.64(4)				
<Ca4–O>	2.43	C7–O18	1.18(4)		
		C7–O19 ×2	1.30(3)		
Ca5–O2	2.35(2)	<C7–O>	1.26		
Ca5–O14	2.35(2)				
Ca5–O12	2.38(2)				
Ca5–O6	2.39(2)				
Ca5–O11	2.40(2)				
Ca5–O4	2.41(2)				
Ca5–OW5	2.51(2)				
<Ca5–O>	2.40				

least one of these sites may be incorrect; (2) the OW7–H7A···OW8 hydrogen bond, with a bond strength of 0.21 valence units, seems unlikely because OW8 would be highly oversaturated in bond strength; and (3) at least one of the three hydrogen bonds received by OW10 is probably incorrect because it is otherwise very oversaturated.

For pseudomarkeyite, all atoms were located and successfully refined at full occupancies to provide a very reasonable structure model; however, because of the aforementioned problems, only the Ca and U atoms could be refined with anisotropic displacement parameters and hydrogen atom sites could not be located. While the general structure is clearly correct, the aforementioned twinning and high mosaicity led to some bond-length anomalies, which we consider refinement artefacts. In particular, some bond lengths are significantly shorter than normal: C5–O13 (1.19 Å), C7–O18 (1.18 Å) and U3–O24 (1.72 Å).

Data collection and refinement details are given in Table 4. Atom coordinates and displacement parameters are given in Tables 5 and 6 for natromarkeyite and pseudomarkeyite, respectively. Selected bond distances are in Tables 7 and 8 for natromarkeyite and pseudomarkeyite, respectively. Bond-valence analyses are in Tables 9 and 10 for natromarkeyite and pseudomarkeyite, respectively. Note that the bond-valence analysis for pseudomarkeyite does not include hydrogen-bond contributions because of the difficulty in proposing an unambiguous hydrogen-bonding scheme for such a complex structure without hydrogen atom positions.

For natromarkeyite, all non-hydrogen atoms were successfully refined with anisotropic displacement parameters. Difference-Fourier synthesis located the hydrogen atom positions related to OW1 to OW7; however, no geometrically reasonable H positions could be found for OW8 to OW11. This could be because of disorder for these H$_2$O groups. The located H-atom positions were refined with soft restraints of 0.82(2) Å on the O–H distances and 1.30(2) Å on the H–H distances and with the U_{eq} of each H set to 1.2 times that of its donor O atom. Hydrogen bonds for OW8 to OW11 are proposed based upon O–O distances and geometries. It should be further noted that, because of the presence of considerable unresolved residual electron density, the assignment of H atom positions related to OW1 to OW7 was difficult and some anomalies suggest that several assignments are questionable: (1) The distance between the H1B and H2B sites is unusually short (1.47 Å), so that at

Table 9. Bond valence analysis for natromarkeyite. Values are expressed in valence units.*

	Ca1	Ca2	Na1	Na2	U1	U2	C1	C2	C3	C4	C5	Donated H bonds	Accepted H bonds	Sum
O1	0.33	0.17					1.46							1.96
O2	0.28				$0.40^{\times2\downarrow}$		1.31							1.99
O3		0.30			$0.46^{\times2\downarrow}$		1.25							2.02
O4	0.33							1.40					0.16, 0.15	2.05
O5						$0.45^{\times2\downarrow}$		1.31					0.21, 0.11	2.08
O6	0.28					$0.41^{\times2\downarrow}$		1.29						1.99
O7			$0.22^{\times2\downarrow}$						1.45				$0.15^{\times2}$	1.98
O8	0.35					$0.45^{\times2\downarrow}$			$1.29^{\times2\downarrow}$					2.09
O9			$0.09^{\times2\downarrow}$							1.53			$0.14^{\times2}$	1.89
O10	0.33				$0.46^{\times2\downarrow}$					$1.24^{\times2\downarrow}$				2.03
O11				$0.16^{\times2\downarrow}$	1.71								$0.10^{\times2}$	2.07
O12					1.79								$0.13^{\times2}$	2.04
O13						1.76							$0.12^{\times2}$	2.00
O14						1.75							0.12	1.87
O15		$0.31^{\times2\rightarrow}$									$1.50^{\times2\downarrow}$			2.12
O16		$^{\times\frac{1}{2}\downarrow}0.33^{\times2\rightarrow}$									1.22		0.10	1.97
OW1		0.29										−0.21, −0.17		−0.10
OW2	0.23											−0.14, −0.15	0.17	0.11
OW3				$0.25^{\times2\downarrow}$								−0.11, *−0.20*	0.14	0.09
OW4		0.27										−0.16, −0.14		−0.03
OW5		$0.16^{\times2\rightarrow}$										−0.11, *−0.20*		0.02
OW6		0.31										−0.15, −0.13		0.03
OW7		$^{\times\frac{1}{2}\downarrow}0.14^{\times2\rightarrow}$										−0.21, −0.12		−0.05
OW8				0.26								−0.10, −0.10	0.21	0.27
OW9			0.16									−0.10, −0.10		−0.04
OW10												−0.13, −0.12	0.11, 0.13, 0.15	0.14
OW11			0.30									−0.15, −0.15		0.00
Sum	2.13	2.05	1.08	1.08	6.14	6.13	4.02	4.00	4.03	4.01	4.23			

* Multiplicity is indicated by ×↓→. Bond-valence parameters from Gagné and Hawthorne (2015); hydrogen-bond strengths based on O–O bond lengths from Ferraris and Ivaldi (1988). Donated hydrogen-bond strengths are shown as negative values. There was no obvious hydrogen-bond receptor for one H atom of the OW3 and the OW5 group; assuming that these H atoms donate multiple weak hydrogen bonds, a donated bond strength of −0.20 (shown in italics) is assigned to OW3 and OW5.

Description and discussion of the structures

The structures of markeyite, natromarkeyite and pseudomarkeyite are constructed of similar components. The U sites in the structures are surrounded by eight O atoms forming a squat UO_8 hexagonal bipyramid. These bipyramids are each chelated by three CO_3 groups, forming a uranyl tricarbonate cluster (UTC) of formula $[(UO_2)(CO_3)_3]^{4-}$ (Fig. 6). As noted by Burns (2005), UTCs are especially common structural features in uranyl carbonates that crystallise from alkaline solutions.

Natromarkeyite

Two independent U sites (U1 and U2) in the structure of natromarkeyite centre two UO_8 hexagonal bipyramids, which combine with CO_3 groups centred by four independent C sites (C1, C2, C3 and C4) to form two different UTCs. As was noted in the structure of markeyite, there is an additional CO_3 group (centred by C5) that is not chelated to a UO_8 hexagonal bipyramid. The $C5O_3$ group is half-occupied, shares an O15–O15 edge with an equivalent $C5O_3$ group and is completed by a half-occupied O16 site. Due to steric limitations, only one of the adjacent C5 sites can be occupied at the same time. Another half-occupied O site (OW7) is located 1.28 Å from the O16 site and cannot be occupied when the O16 site is occupied. There are two different Ca–O polyhedra in the structure. Ca1 bonds to seven fully occupied O sites, Ca2 bonds to seven fully occupied and two half-occupied O sites for a total effective coordination of eight. The Na1 occupies a position equivalent to the Ca3 site in the markeyite structure, while the Na2 site has no counterpart in the markeyite structure. Na1 is octahedrally coordinated to five fully occupied O sites and one O site (OW11) with a refined occupancy of 0.96 that can be considered essentially fully occupied. Na2 bonds to five fully occupied O sites forming a $Na2O_5$ trigonal bipyramid.

The two Ca–O polyhedra share edges and corners with the UTCs in very different ways. The $Ca1O_7$ polyhedra share edges with U1 and U2 bipyramids and corners with $C1O_3$ and $C2O_3$ triangles in different UTCs. Pairs of $Ca2O_8$ polyhedra share an edge to form a dimer, which is linked to a second dimer through the half-occupied $C5O_3$ triangles and OW7 sites. The group of four $Ca2O_8$ polyhedra (with the $C5O_3$ triangle at its centre) is linked to two U1 UTCs by edge sharing between $Ca2O_8$ polyhedra and $C1O_3$ triangles. The $Na1O_6$ octahedra share corners with two $C3O_3$ and two $C4O_3$ triangles, each belonging to independent UTC units. The $Na2O_5$ trigonal bipyramids share their apical vertices (O11) with apical (uranyl) vertices of two symmetrically related U1 hexagonal bipyramids. The linkages between the Ca and Na polyhedra and the UTCs form thick corrugated heteropolyhedral layers parallel to {010} (Fig. 7) and these layers link to one another and to interlayer H_2O groups (OW10) only *via* hydrogen bonds (Fig. 8). This explains the perfect {010} cleavage.

As noted above, the Na2 site in the natromarkeyite structure has no counterpart in the markeyite structure. The OW3 and OW8 groups, which are coordinated to Na2 in natromarkeyite, are interlayer H_2O sites in markeyite. Additionally, there is a partially occupied OW12 site bonded to Ca3 in the markeyite structure, which has no counterpart in the natromarkeyite structure. Summing the H_2O site occupancies in the two structures provides

Table 10. Bond valence analysis for pseudomarkeyite. Values are expressed in valence units.*

	Ca1	Ca2	Ca3	Ca4	Ca5	U1	U2	U3	C1	C2	C3	C4	C5	C6	C7	Sum
O1		0.32				0.44			1.34							2.10
O2					0.34	0.44			1.38							2.16
O3				0.32×2↓					1.38							1.70
O4					0.29					1.49						1.78
O5	0.30						0.50			1.34						2.14
O6					0.31	0.41				1.22						1.94
O7		0.33									1.52					1.85
O8		0.23					0.43				1.31					1.97
O9	0.29						0.49				1.19					1.97
O10							0.44×2↓					1.41				1.85
O11					0.30		0.41×2↓					1.52				2.23
O12	0.29				0.31							1.28				1.88
O13				0.39									1.68			2.07
O14					0.34		0.43×2↓						1.22×2↓			1.99
O15		0.33						0.44×2↓						1.52		2.29
O16			0.35×2↓					0.45×2↓						1.22		2.02
O17		0.37												1.25		1.62
O18				0.41											1.73	2.14
O19		0.23						0.45×2↓							1.28×2↓	1.96
O20						1.79										1.79
O21						1.72										1.72
O22							1.83									1.83
O23							1.58									1.58
O24								1.99								1.99
O25								1.75								1.75
OW1	0.25															0.25
OW2				0.22×2↓												0.22
OW3	0.31															0.31
OW4				0.17												0.17
OW5	0.27				0.23											0.50
OW6		0.19														0.19
OW7	0.28															0.28
OW8			0.26													0.26
OW9			0.34×2↓													0.34
OW10			0.31×2↓													0.31
OW11																0.00
OW12																0.00
Sum	1.99	2.01	2.24	2.06	2.12	6.32	5.96	6.45	4.10	4.05	4.02	4.21	4.12	3.99	4.29	

* Multiplicity is indicated by ×2↓. Bond valence parameters from Gagné and Hawthorne (2015). Hydrogen-bond contributions are not included.

27.30 H_2O pfu (ideally 27) for natromarkeyite and 28.25 H_2O pfu (ideally 28) for markeyite. Expressing the structurally bound H_2O groups (those bonded to cations) separately from the isolated H_2O groups (those linked only *via* hydrogen bonds), results in the ideal formulas $Ca_9(UO_2)_4(CO_3)_{13}(H_2O)_{22} \cdot 6H_2O$ for markeyite and $Na_2Ca_8(UO_2)_4(CO_3)_{13}(H_2O)_{24} \cdot 3H_2O$ for natromarkeyite. In spite of their minor structural differences, markeyite and natromarkeyite are considered essentially isostructural.
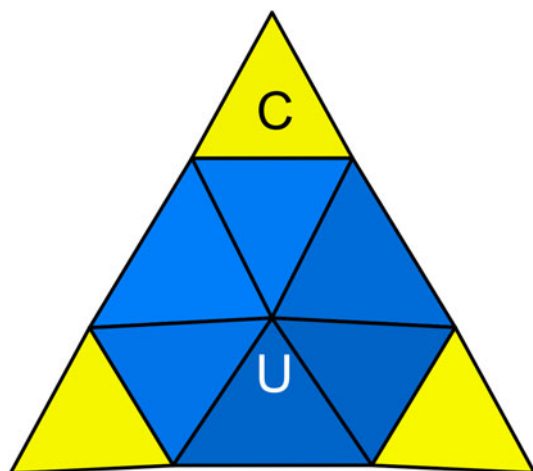

Fig. 6. The uranyl tricarbonate cluster (UTC) of formula $[(UO_2)(CO_3)_3]^{4-}$ consisting of a squat UO_8 bipyramid and three CO_3 groups sharing alternating UO_8 equatorial edges.

Pseudomarkeyite

The three U sites (U1, U2 and U3) in the structure of pseudomarkeyite centre three UO_8 hexagonal bipyramids, which coordinate to CO_3 groups centred by seven independent C sites (C1 to C7) to form three different UTCs. There is no additional non-UTC CO_3 group in the pseudomarkeyite structure. Five Ca–O polyhedra share edges and corners with the UTCs. The UTCs and Ca–O polyhedra form thick corrugated heteropolyhedral layers parallel to {10$\bar{1}$}. These layers are very similar to the layers in markeyite (Fig. 6), but differ in several respects. The most obvious difference is that the pseudomarkeyite layer is missing the distinctive grouping of four Ca2 polyhedra (and C5 triangle) found in the markeyite layer. Viewed down the **b** axis (Fig. 8), another important difference in the structures is evident. In the markeyite structure, the heteropolyhedral layers link to one another and to interlayer H_2O groups only *via* hydrogen bonds; however, in the pseudomarkeyite structure, the layers are linked through edge and corner links to Ca polyhedra.
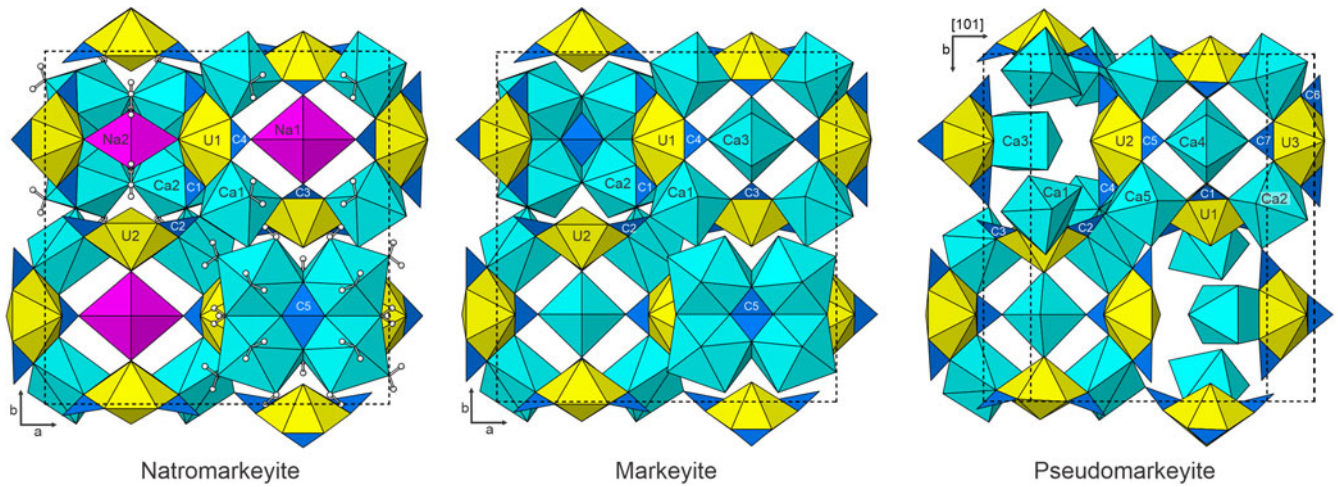
Fig. 7. The heteropolyhedral layers in markeyite, natromarkeyite and pseudomarkeyite. The polyhedra are labelled and for natromarkeyite the H atoms are shown as small white spheres. The unit cells are outlined with dashed lines.
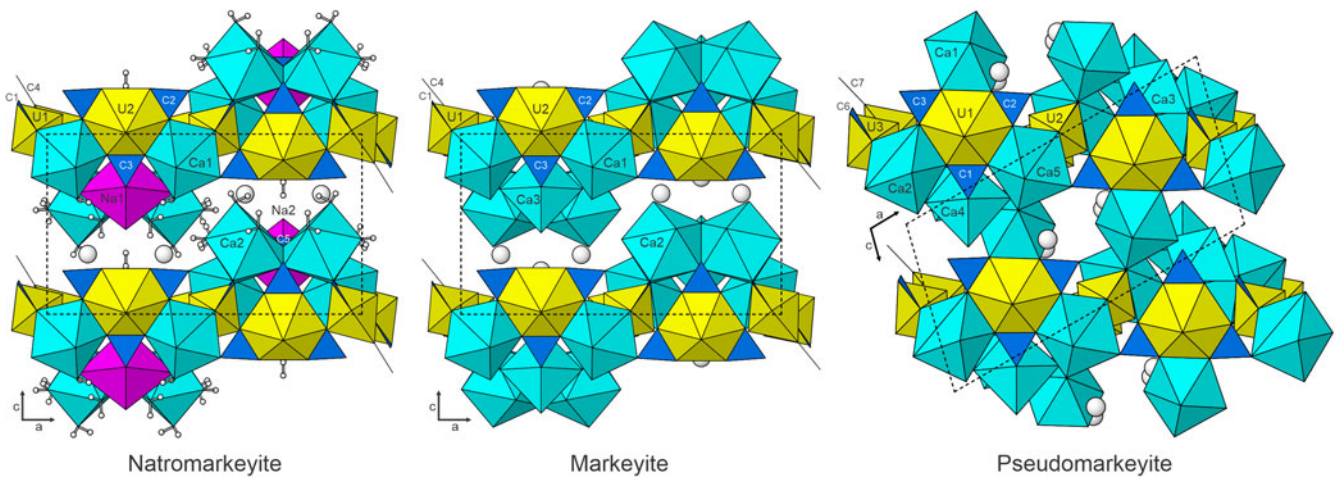
Fig. 8. The structures of markeyite, natromarkeyite and pseudomarkeyite viewed down [010] with heteropolyhedral layers horizontal. The polyhedra are labelled, the O atoms of the isolated H_2O groups are shown as large white spheres and H atoms for natromarkeyite are shown as small white spheres. The unit cells are outlined with dashed lines.
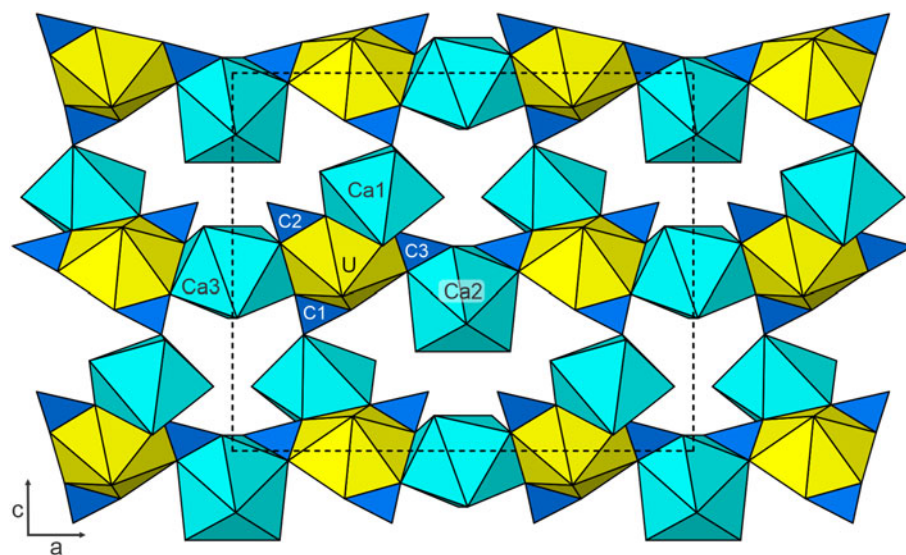
Fig. 9. Heteropolyhedral layer in the structure of liebigite viewed down [010]. The unit cell is outlined with dashed lines.

Table 11. Information measures for selected uranyl carbonates.

Mineral	V (Å³)	v	I_G (bits/atom)	$I_{G,total}$ (bits/cell)	$I_{chem, norm.}$ (bits/formula/Z)
Liebigite	4015.8	200	5.664	1132.77	9.90
Pseudomarkeyite	2882.3	270	6.218	1678.74	114.21
Natromarkeyite	3346.6	302	5.583	1686.00	135.54
Markeyite	3356.6	340	5.833	1938.19	134.27

v = number of atoms in the reduced unit cell.
I_G = structural information content.
I_{chem} = chemical information content normalised by Z.

Another interesting contrast relates to the edges shared between UO₈ bipyramids and Ca polyhedra. Note that in any UTC, the UO₈ bipyramid has three equatorial edges that are not shared with CO₃ groups. In the markeyite and natromarkeyite structures, each of the two UO₈ bipyramids shares two of these equatorial edges with Ca polyhedra, the third equatorial edge being unshared. In the pseudomarkeyite structure, the U1 and U3 bipyramids share all three available non-CO₃ equatorial edges with Ca polyhedra, while the U2 bipyramid shares only two such edges.

Comparison with other structures

Lussier *et al.* (2016) provide a review of inorganic uranyl compounds that includes specifics of the structures of uranyl carbonate minerals. Their review shows the UTC structural unit to be a prominent feature in the majority of uranyl carbonate minerals. In these structures, the UTCs are linked by various combinations of counter cations and hydrogen-bonding networks as 0-dimensional clusters. These are usually incorporated into heteropolyhedral sheets, such as in the minerals liebigite (Mereiter, 1982), grimselite (Plášil *et al.*, 2012) and línekite (Plášil *et al.*, 2017). There are also complex clusters, such as those in ewingite (Olds *et al.*, 2017b) and paddlewheelite (Olds *et al.*, 2018), which combine UTCs with other building units, such as the trimers of uranyl polyhedra in ewingite and the square–pyramidal copper polyhedra in paddlewheelite. Less commonly, the structural units in uranyl carbonate minerals are infinite sheets of uranyl polyhedra and carbonate triangles, such as in rutherfordine (Finch *et al.*, 1999), fontanite (Hughes and Burns, 2003), sharpite (Plášil, 2018) and meyrowitzite (Kampf *et al.*, 2019e), and sheets containing also lanthanide-centred polyhedra, such as in bijvoetite-(Y) and kamotoite-(Y) (Plášil and Petříček, 2017).

The uranyl carbonate mineral with which the structures of markeyite, natromarkeyite and pseudomarkeyite are most similar is liebigite, Ca₂(UO₂)(CO₃)₃·11H₂O (Mereiter, 1982). All four structures contain the same structural components and the same types of polyhedral linkages. In all four, the Ca–O polyhedra link the UTCs forming thick corrugated heteropolyhedral layers. In the structure of liebigite, as in those of markeyite, natromarkeyite and natromarkeyite, these layers link to one another and to interlayer H₂O groups only *via* hydrogen bonds; however, the topology of the layer in liebigite (Fig. 9) is quite different from those in markeyite, natromarkeyite and pseudomarkeyite.

Structural complexity

We examined the structural complexity of markeyite, natromarkeyite and pseudomarkeyite, as well as that of the related mineral liebigite. As developed by Krivovichev (2012, 2013, 2014, 2018), structural complexity can be quantified as the total structural information content, $I_{G,total}$. As available structure determinations of liebigite, markeyite and pseudomarkeyite lack H atom positions, the approximate calculations of the fictive H atoms contribution to the total structure complexity were undertaken. An overview of the structural and chemical complexity measures of the four minerals, calculated using the program TOPOS (Blatov *et al.*, 2014), is given in Table 11.

Both structurally and chemically, the least complex is liebigite, which represents a 'relatively simple' layered structure. The structures of markeyite, natromarkeyite and pseudomarkeyite are significantly more complex, owing to the additional linkages (e.g. the Ca2–C5O₃–C5O₃–Ca2 linkages in markeyite). These three structures are nearly as complex as the suite of complex uranyl carbonate structures based upon 'paddle-wheel' units, which have $I_{G,total}$ >2000 bits/unit cell: braunerite, K₂Ca(UO₂)(CO₃)₃·6H₂O (Plášil *et al.*, 2016), línekite, K₂Ca₃[(UO₂)(CO₃)₃]₂·7H₂O (Plášil *et al.*, 2017) and paddlewheelite, MgCa₅Cu₂(UO₂)₄(CO₃)₁₂·33H₂O (Olds *et al.*, 2018). The most structurally complex uranyl carbonate mineral, ewingite, Mg₈Ca₈(UO₂)₂₄(CO₃)₃₀O₄(OH)₁₂·180H₂O (Olds *et al.*, 2017b), is also the most structurally complex mineral known.

Given the similarities in the structures of markeyite, natromarkeyite and pseudomarkeyite, it is not surprising that their structural complexities are very similar. The chemical complexity ($I_{chem, norm.}$) of natromarkeyite is somewhat higher due to incorporation of an additional cation in the structure. These minerals certainly form under similar conditions, although natromarkeyite is found in in assemblages more enriched in Na, typically including the mineral andersonite.

References

Anderson A., Chieh Ch., Irish D.E. and Tong J.P.K. (1980) An X-ray crystallographic, Raman, and infrared spectral study of crystalline potassium uranyl carbonate, K₄UO₂(CO₃)₃. *Canadian Journal of Chemistry*, **58**, 1651–1658.

Bartlett J.R. and Cooney R.P. (1989) On the determination of uranium–oxygen bond lengths in dioxouranium(VI) compounds by Raman spectroscopy. *Journal of Molecular Structure*, **193**, 295–300.

Blatov V.A, Shevchenko, A.P. and Proserpio, D.M. (2014) Applied topological analysis of crystal structures with the program package ToposPro. *Crystal Growth and Design*, **14**, 3576–3586.

Burla M.C., Caliandro R., Camalli M., Carrozzini B., Cascarano G.L., Giacovazzo C., Mallamo M., Mazzone A., Polidori G. and Spagna R. (2012) SIR2011: a new package for crystal structure determination and refinement. *Journal of Applied Crystallography*, **45**, 357–361.

Burns P.C. (2005) U⁶⁺ minerals and inorganic compounds: insights into an expanded structural hierarchy of crystal structures. *The Canadian Mineralogist*, **43**, 1839–1894.

Čejka J. (1999) Infrared and thermal analysis of the uranyl minerals. Pp. 521–622 in: *Uranium: Mineralogy, Geochemistry, and the Environment* (P.C. Burns and R. Finch, editors). Reviews in Mineralogy, **38**. Mineralogical Society of America, Washington, DC.

Čejka J. (2005) Vibrational spectroscopy of the uranyl minerals – infrared and Raman spectra of the uranyl minerals. II. Uranyl carbonates. *Bulletin mineralogicko–petrologického oddělení Národního muzea (Praha)*, **13**, 62–72 [in Czech].

Chenoweth W.L. (1993) The geology and production history of the uranium deposits in the White Canyon mining district, San Juan County, Utah. *Utah Geological Survey Miscellaneous Publication*, 93–3.

Ferraris G. and Ivaldi G. (1988) Bond valence vs. bond length in O···O hydrogen bonds. *Acta Crystallographica*, **B44**, 341–344.

Finch, R.J., Cooper, M.A., Hawthorne, F.C. and Ewing, R.C. (1999) Refinement of the crystal structure of rutherfordine. *The Canadian Mineralogist*, **37**, 929–938.

Gagné O.C. and Hawthorne F.C (2015) Comprehensive derivation of bond-valence parameters for ion pairs involving oxygen. *Acta Crystallographica*, **B71**, 562–578.

Gunter M.E., Bandli B.R., Bloss F.D., Evans S.H., Su S.C. and Weaver R. (2004) Results from a McCrone spindle stage short course, a new version of EXCALIBR, and how to build a spindle stage. *The Microscope*, **52**, 23–39.

Higashi T. (2001) *ABSCOR*. Rigaku Corporation, Tokyo.

Hughes, K.-A. and Burns, P.C. (2003) A new uranyl carbonate sheet in the crystal structure of fontanite, $Ca[(UO_2)_3(CO_3)_2O_2](H_2O)_6$. *American Mineralogist*, **88**, 962–966.

Kampf A.R., Plášil J., Kasatkin A.V., Marty J. and Čejka J. (2017) Klaprothite, péligotite and ottohahnite, three new sodium uranyl sulfate minerals with bidentate UO_7–SO_4 linkages from the Blue Lizard mine, San Juan County, Utah, USA. *Mineralogical Magazine*, **81**, 753–779.

Kampf A.R., Plášil J., Kasatkin A.V., Marty J. and Čejka J. (2018) Markeyite, a new calcium uranyl tricarbonate mineral from the Markey mine, San Juan County, Utah, USA. *Mineralogical Magazine*, **82**, 1089–1100.

Kampf, A.R., Olds, T.A., Plášil, J., Burns, P.C. and Marty, J. (2019a) Pseudomarkeyite, IMA 2018-114. CNMNC Newsletter No. 47, February 2019, page 144; *Mineralogical Magazine*, **83**, 143–147.

Kampf, A.R., Olds, T.A., Plášil, J., Marty, J. and Burns, P.C. (2019b) Natromarkeyite, IMA 2018-152. CNMNC Newsletter No. 48, April 2019, page 316; *Mineralogical Magazine*, **83**, 315–317.

Kampf A.R., Olds T.A., Plášil J., Marty J. and Perry S.N. (2019c) Feynmanite, a new sodium–uranyl–sulfate mineral from Red Canyon, San Juan County, Utah, USA. *Mineralogical Magazine*, **83**, 153–160.

Kampf A.R., Plášil J., Kasatkin A.V., Nash B.P. and Marty J. (2019d) Magnesioleydetite and straßmannite, two new uranyl sulfate minerals with sheet structures from Red Canyon, Utah. *Mineralogical Magazine*, **83**, 349–360.

Kampf A.R., Plášil J., Olds T.A., Nash B.P., Marty J. and Belkin H.E. (2019e) Meyrowitzite, $Ca(UO_2)(CO_3)_2 \cdot 5H_2O$, a new mineral with a novel uranyl–carbonate sheet. *American Mineralogist*, **103**, 603–610.

Kampf A.R., Plášil J., Nash B.P., Němec I. and Marty J. (2020) Uroxite and metauroxite, the first two uranyl–oxalate minerals. *Mineralogical Magazine*, **84**, 131–141.

Koglin E., Schenk H.J. and Schwochau K. (1979) Vibrational and low temperature optical spectra of the uranyl tricarbonato complex $[UO_2(CO_3)_3]^{4-}$. *Spectrochimica Acta*, **35A**, 641–647.

Krivovichev, S.V. (2012) Topological complexity of crystal structures: quantitative approach. *Acta Crystallographica*, **A68**, 393–398.

Krivovichev, S.V. (2013) Structural complexity of minerals: information storage and processing in the mineral world. *Mineralogical Magazine*, **77**, 275–326.

Krivovichev, S.V. (2014) Which inorganic structures are the most complex? *Angewandte Chemie International Edition*, **53**, 654–661.

Krivovichev, S.V. (2018) Ladders of information: what contributes to the structural complexity of inorganic crystals. *Zeitschrift für Kristallographie*, **233**, 155–161.

Libowitzky E. (1999) Correlation of O–H stretching frequencies and O–H···O hydrogen bond lengths in minerals. *Monatshefte für Chemie*, **130**, 1047–1059.

Lussier A.J., Lopez R.A. and Burns P.C. (2016) A revised and expanded structure hierarchy of natural and synthetic hexavalent uranium compounds. *The Canadian Mineralogist*, **54**, 177–283.

Mandarino J.A. (1976) The Gladstone–Dale relationship – Part 1: derivation of new constants. *The Canadian Mineralogist*, **14**, 498–502.

Mandarino J.A. (2007) The Gladstone–Dale compatibility of minerals and its use in selecting mineral species for further study. *The Canadian Mineralogist*, **45**, 1307–1324.

Mereiter K. (1982) The crystal structure of liebigite, $Ca_2UO_2(CO_3)_3 \cdot \sim 11H_2O$. *Tschermaks Mineralogische und Petrographische Mitteilungen*, **30**, 277–288.

Olds T., Sadergaski L.R., Plášil J., Kampf A.R., Burns P., Steele I.M., Marty J., Carlson S.M. and Mills O.P. (2017a) Leószilárdite, the first Na,Mg–containing uranyl carbonate from the Markey Mine, San Juan County, Utah, USA. *Mineralogical Magazine*, **81**, 743–754.

Olds T.A., Plášil J., Kampf A.R., Simonetti A., Sadergaski L.R., Chen Y.-S. and Burns P.C. (2017b) Ewingite: Earth's most complex mineral. *Geology*, **45**, 1007–1010.

Olds T.A., Plášil J., Kampf A.R., Dal Bo F. and Burns P.C. (2018) Paddlewheelite, a new uranyl carbonate from the Jáchymov District, Bohemia, Czech Republic. *Minerals*, **8**, 511.

Plášil, J. (2018) A unique structure of uranyl-carbonate mineral sharpite: a derivative of the rutherfordine topology. *Zeitschrift für Kristallographie*, **233**, 579–586.

Plášil, J. and Petříček, V. (2017) Crystal structure of the (REE)-uranyl carbonate mineral kamotoite-(Y). *Mineralogical Magazine*, **81**, 653–660.

Plášil, J., Fejfarová, K., Skála, R., Škoda, R., Meisser, N., Hloušek, J., Císařová, I., Dušek, M., Veselovský, F., Čejka, J., Sejkora, J. and Ondruš, P. (2012) The crystal chemistry of the uranyl carbonate mineral grimselite, $(K,Na)_3Na[(UO_2)(CO_3)_3](H_2O)$, from Jáchymov, Czech Republic. *Mineralogical Magazine*, **76**, 446–453.

Plášil, J., Mereiter K., Kampf A.R., Hloušek J., Škoda R., Čejka J., Nˇemec I. and Ederová J. (2016) Braunerite, IMA2015-123. CNMNC Newsletter No. 31, June 2016, page 692; *Mineralogical Magazine*, **80**, 691–697.

Plášil, J., Čejka J., Sejkora J., Hloušek J., Škoda R., Novák M., Dušek M., Císařová I., Němec I. and Ederová J. (2017) Línekite, $K_2Ca_3[(UO_2)(CO_3)_3]_2 \cdot 8H_2O$, a new uranyl carbonate mineral from Jachymov, Czech Republic. *Journal of Geosciences*, **62**, 201–213.

Pouchou J.-L. and Pichoir F. (1991) Quantitative analysis of homogeneous or stratified microvolumes applying the model "PAP." Pp. 3l–75 in: *Electron Probe Quantitation* (K.F.J. Heinrich and D.E. Newbury, editors). Plenum Press, New York.

Sheldrick G.M. (2015) Crystal structure refinement with *SHELX*. *Acta Crystallographica*, **C71**, 3–8.